JMEPEG (2017) 26:4166–4176
DOI: 10.1007/s11665-017-2853-x

1059-9495/$19.00

Prospects of In-Situ α-Al_2O_3 as an Inoculant in Aluminum: A Feasibility Study

V.M. Sreekumar, N. Hari Babu, and D.G. Eskin

(Submitted March 20, 2017; in revised form May 31, 2017; published online August 21, 2017)

In-situ α-Al_2O_3 was successfully synthesized and dispersed in Al alloy using B_2O_3 and ultrasonication-aided liquid mixing technique. Microstructure analysis identified α-Al_2O_3 as the most common phase in the composite master alloy, whereas AlB_{12} was frequently observed and AlB_2 was rarely found in the alloy. Grain refinement analysis of selected Al alloys registered a transition of columnar to equiaxial grains of α-Al with the inoculation of the master alloy and ultrasonication treatment. Similarly, an improvement in the mechanical properties of A357 alloy was observed with the combination of inoculation and ultrasonication treatment.

Keywords grain refinement, in situ composites, ultrasonic cavitation, α-Al_2O_3

1. Introduction

Oxides are high melting point ceramic compounds having special physical and mechanical properties. Al_2O_3, SiO_2, alumina silicate, flyash are a few examples of oxides commonly used as reinforcements (fibers, whiskers, particles, etc.) in metal–ceramic composites in order to increase the strength and creep properties of the alloy (Ref 1). A simpler and economical liquid metallurgy technique (impeller mixing or stir casting) is widely used to disperse the oxides in liquid Al. Usually in all metal–ceramic composite systems, wettability is one of the important factors that define the interfacial bonding and load transfer properties between metal and reinforcement (Ref 1, 2). While looking at the wettability properties of different ceramic materials, oxides are the worst performing because of the high contact angle (wetting angle) that forms with molten Al (Ref 1). Hence, establishing wettability between oxides and molten Al is challenging, even more in the case of composite manufacturing through stir casting process. Lack of wetting often results in clustering and rejection of particles in the molten metal while mixing by an impeller (Ref 3). Wettability properties of oxides with aluminum are generally improved by changing the composition of Al with the addition of elements like Mg, Cu, Ti, etc., where Mg is found as the most successful wetting agent (surfactant) (Ref 1-4). Mg has another role as the scavenger of oxygen entrapped inside the pores of the particles by nature or during mixing (Ref 3).

For the past decades, Al_2O_3, $MgAl_2O_4$, and MgO compounds were investigated as the interfacial reaction phases in oxide reinforced Al MMCs (Ref 5-9). In effect, these interfacial products improve the wetting and prevent the degradation of reinforcement (Ref 1). In recent times, research on the composites is essentially concentrated on the in situ formation of these phases as reinforcements at high percentage (in situ MMCs). Among the various processes established until now, the displacement reactions between the liquid metal and the ceramic oxides are found to gain interest, because of the thermodynamic feasibility of the reactions at the experimental conditions (Ref 10). The materials such as SiO_2, CuO, TiO_2 are recognized as the volatile ceramic oxides amenable for the in situ generation of Al_2O_3, $MgAl_2O_4$, and MgO in Al alloy (Ref 5, 9, 11). The Al_2O_3-$MgAl_2O_4$-MgO phase equilibria (reflective of volatile oxides dispersed in liquid Al) were studied by thermodynamic models and experimentally verified with different Mg composition of matrix alloy elsewhere (Ref 12). The studies established that Al_2O_3 is stable at Mg content <0.19 wt.%, whereas $MgAl_2O_4$ is stable between 0.007 and 10 wt.% Mg and MgO is stable at >7 wt.% Mg (Ref 12). While volatile oxides enable the in situ oxide particle formation in Al, the dispersion of volatile oxides (by impeller) is found difficult without any wetting agent. More often, a successful dispersion of the volatile oxides in Al is achieved by more Mg-containing Al alloy. This means that the formation of Al_2O_3 as in situ phase in molten Al becomes less feasible. As a matter of fact, in situ Al_2O_3 dispersion in liquid Al by stir casting technique is not reported; however, studies are available in Al-oxide powder compacts and infiltration of pure aluminum in oxide preforms (Ref 13, 14).

Recently, grain refinement was reported in oxide-containing Al alloys. Atamanenko et al. (Ref 15) looked at the grain refinement of pure Al possibly by ultrasonic cavitation-induced heterogeneous nucleation through the activation of externally added Al_2O_3 particles. Li et al. (Ref 16) and Kim (Ref 17) demonstrated grain refinement of Al-Mg alloys using an intensive melt shearing technique and proposed a mechanism related to heterogeneous nucleation of Al on naturally occurring $MgAl_2O_4$ or MgO particles in Al alloys. Sreekumar et al. (Ref 5) observed an appreciable reduction in grain size in Al-Mg-$MgAl_2O_4$ in situ composite possibly by the presence of in situ $MgAl_2O_4$. Further, Sreekumar et al. systematically examined grain refining potency and efficiency of $MgAl_2O_4$ in Al alloys by a master alloy method (Ref 18). Even though Al_2O_3 phase is present naturally (in situ) in Al aplenty, no reports are available on the grain refinement of Al using in situ Al_2O_3 particles as inoculants.

V.M. Sreekumar, N. Hari Babu, and **D.G. Eskin**, BCAST, Brunel University London, London UB8 3PH, UK. Contact e-mail: Sreekumar.VadakkeMadam@brunel.ac.uk.

For the first time in author's knowledge, this paper reports on a technique for the synthesis and dispersion of in situ α-Al_2O_3 in liquid Al. Being an important oxide phase that is present in Al, grain refinement potential of α-Al_2O_3 in Al alloys is examined by a master alloy method. The composite is used as the master alloy for the grain refinement experiments in commercial and model Al alloys. Mechanical properties of one of the commercial Al alloys are examined after the inoculation technique.

2. Materials and Methods

Commercially pure Al (CPAl, 0.08 wt.% Si, 0.1 wt.% Fe, remaining Al) and B_2O_3 were taken as starting materials. The initial particle size of B_2O_3 supplied from Sigma-Aldrich was in the range of 30-70 μm. B_2O_3 powder undergoes crystallographic changes at higher temperatures and subsequently melts at 440 °C to form a glassy structure. Hence, B_2O_3 particles immediately transform to viscous liquid inside the molten metal. Added to that, the density of B_2O_3 changes from 2.5 to 1.8 g/cc after the melting point, which is less than the density of liquid aluminum (2.3 g/cc). Initially, the alloys were melted and treated in a boron nitride-coated clay graphite crucible at a temperature between 700 and 900 °C. B_2O_3 particles were mixed using a mechanical impeller made from Ti alloy and coated with a high temperature ceramic glue to minimize impeller erosion during processing. The metal was ultrasonicated (water-cooled magnetostrictive system, Realtec, Russia, 17.5 kHz, 3.5 kW, 40-μm peak-to-peak amplitude, Nb sonotrode) to ensure the dispersion of particles and the completion of reaction. The Al_2O_3 content in the cast sample [referred to as master alloy (MA)] was approximated using reaction (1) shown later in the paper.

Grain refinement assessment was conducted on a commercial alloy (A357-7.4 wt.% Si, 0.5 wt.% Mg, 0.1 wt.% Fe, 0.1 wt.% Ti, remaining Al) and model alloys (CPAl and Al-1Si-0.5 Mg alloys). The master alloy was added to 300 g of molten alloy at 760 °C and cast at 750 °C in a steel mold (cooling rate ~2 °C/s) preheated to 250 °C before casting (Fig. 1). In some experiments, the alloys were treated with ultrasound for 3 min at 740-750 °C before casting (ultrasonic processing parameters were the same as shown above for the master alloy). In all the cases, cast samples were ground using SiC paper (400-2500-grid size) and polished using OPS. For identification of grain size, polished samples were anodized using 4% HBF_4 solution for approximately 1 min at 20 VDC and analyzed in polarized light in an optical microscope (Zeiss Axioscope). Microstructure of the alloys was investigated using optical microscopy (Zeiss Axioscope), and phase identification in the master alloy was performed using x-ray Diffraction (Bruker D8 Advance) and scanning electron microscopy (Zeiss Supra 35VP) coupled with energy-dispersive spectroscopy (EDAX).

Cooling curves of the selected compositions from liquid to solid transformation were measured with K-type thermocouples and recorded by means of dedicated software (NI-LABVIEW Data Logger) collecting 100 data per second. The steel mold used for grain refinement study was preheated to 350 °C and covered with ceramic wool in order to minimize the heat loss. The thermocouple was positioned from the top between the center and the wall of the mold. The 300 g of A357 alloy was poured at a superheat of 100 °C above the liquidus of the alloy (620 °C).

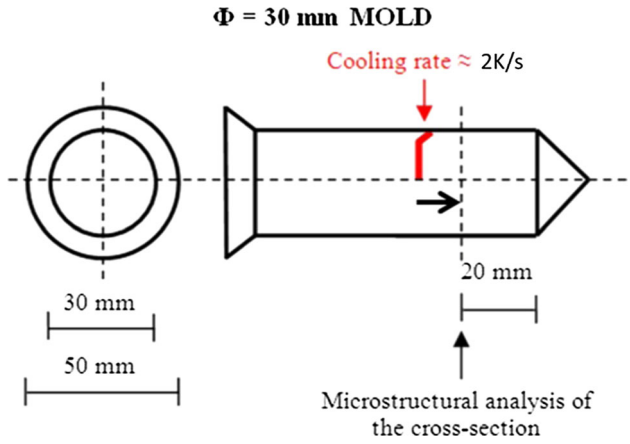

Fig. 1 Schematic of metallic mold used for grain refinement studies

The tensile tests of machined specimens (four samples for each condition) were carried out in Instron 5569 with 50-kN load cell (ASTM E8). The sample dimensions of ASTM standard B557 cylindrical specimen with a gauge length of 25 mm were cast in a permanent steel mold (1-kg melt charge). The casting conditions were kept similar to those of microstructural studies. Prior to testing, all test bars were heat-treated. The samples were solutionized for 12 h at 540 °C, water-quenched (warmed at 50 °C), and subsequently aged at 170 °C for 12 h. Elongation of the samples was recorded using an external extensometer (25-mm gauge length), and the yield stress was calculated by the offset method.

3. Experimental

3.1 Technique to Produce an Al-Al_2O_3 Master Alloy

3.1.1 Mixing of B_2O_3 Particles in CPAl. We started with testing a simple approach. B_2O_3 particles wrapped in Al foil were added to CPAl while impeller was running to form vortex. Glassy B_2O_3 was found to stick on the stirrer initially and floated to the top of the metal subsequently. The metal containing B_2O_3 was held at 900 °C for 30 min and cooled down to 700 °C. Later, the metal was mechanically mixed using impeller at 700-720 °C for 5 min. The holding–mixing cycle was repeated 3-4 times until casting was performed. In another trial, molten CPAl was poured onto the molten B_2O_3 at 750 °C and mixed by ultrasonication for 5 min at 730-750 °C in order to disperse the liquid B_2O_3 directly. Similar to previous trial, holding–mixing was repeated 3-4 times until casting was performed. In both the cases, large lump of viscous B_2O_3 was visibly found separated on the top of the metal before casting. The metal was cut in cross section to find the particles entrapped into the metal. The microstructure shows large B_2O_3 clusters in the metal (Fig. 2a), and close observation of the lump revealed the sign of reaction, where small clusters of product crystals were observed (shown by arrows in Fig. 2b). It was inferred that both methodologies were just good enough for introducing B_2O_3 in Al as some of the B_2O_3 was gone into the metal, but not sufficient to disperse B_2O_3 or reaction products.

3.1.2 Mixing of B_2O_3 in Al-0.4 Mg Alloy. In the third trial, B_2O_3 was mixed using impeller and ultrasonication in an Al-0.4 wt.% Mg alloy. In order to achieve low surface tension and improve wettability with B_2O_3, 0.4 wt.% Mg was added in CPAl initially. 5 wt.% of B_2O_3 particles was stirred in molten Al-0.4 wt.% Mg alloy at temperatures between 650 and 700 °C by an impeller and subsequently ultrasonicated for 5 min at 700-720 °C. The mixed melt was held at 900 °C for 30 min to facilitate the reaction between oxide particles and liquid Al. Subsequently, the temperature was decreased to 700-720 °C and the melt was ultrasonicated for 5 min while impeller was running to ensure the dispersion of reaction product and complete reaction of B_2O_3. The cycles of holding and mixing processes were repeated 3-4 times and cast at 750 °C. The B_2O_3 was introduced much easier, most likely by the presence of Mg that initially stabilized the glassy liquid inside molten Al to facilitate the reaction and later on the dispersion of B_2O_3 and products in mixing–holding cycles.

This method of introduction, reaction, and dispersion of oxides was chosen, and the results are presented below.

4. Results and Discussion

4.1 Reaction Products

The reaction between B_2O_3 and Al can be represented as (Ref 19):

$$2Al + B_2O_3 = \alpha - \ Al_2O_3 + 2B \qquad \text{(Eq 1)}$$

$$\Delta G^{o}_{298} = -416.9 \text{ kJ/mol} \qquad \text{(Eq 2)}$$

$$\Delta H^{o}_{298} = -402.7 \text{ kJ/mol} \qquad \text{(Eq 3)}$$

It is clear that Gibbs free energy of formation of Al_2O_3 from B_2O_3 is negative and an exothermic reaction occurs at the interface between molten Al and B_2O_3. From x-ray diffraction of the master alloy, only α-Al_2O_3 phase and Al were detected (Fig. 3). Since no B_2O_3 was noticed, the reaction (1) was assumed to be completed forming Al_2O_3 and atomic boron (B). According to reaction 1, 5 wt.% of B_2O_3 forms 7.6 wt.% (5.9 vol.%) Al_2O_3 and 1.5 wt.% B. Figure 4 shows the optical micrographs of Al-1.5B-7.6 Al_2O_3 master alloy where a few micrometer-sized particles likely to be Al_2O_3 were found to be distributed in the alloy (represented by arrows). SEM–EDS analysis (Fig. 5) confirmed the compound as Al_2O_3 by the presence of oxygen and aluminum on the particles (shown by arrows). Also large blocky shaped particles of 40-50 μm in size were frequently observed in microstructure (Fig. 4). Usually, matrix Al reacts with boron and forms AlB_2 or AlB_{12} depending on the temperature of processing. The compounds can be differentiated in backscattered SEM, where dark particles relate to AlB_{12}, while light gray ones usually relate to AlB_2. First, large blocky shaped particles were confirmed as boron-bearing compound and further AlB_{12} in backscattered SEM (Fig. 6). The EDS analysis detected Al, Mg, and B on the compound with atomic percentage 7.14, 4.22, and 88.64, and the formation of AlB_{12} compound was confirmed. Interestingly, the result shows a substitutional diffusion of Mg in AlB_{12} likely during the reaction with Al-0.4 Mg alloy and B_2O_3. A mutual diffusion of Al or Mg in AlB_2, AlB_{12}, MgB_2, MgB_{12} as well as the formation of several transition and stable compounds at different conditions was reported in previous studies (Ref 20). In addition to the large particles, fine AlB_{12} particles of 3-4 μm in size were also found in the alloy. Microstructure (Fig. 6) also shows the agglomeration of Al_2O_3 particle yet to be separated apart (shown by arrows). The chains of Al_2O_3 particles are formed at the unstable interface between liquid B_2O_3 and molten Al. Figure 7 shows particle size distribution of Al_2O_3 in the master alloy measured by *Imagej* software. It is very clear

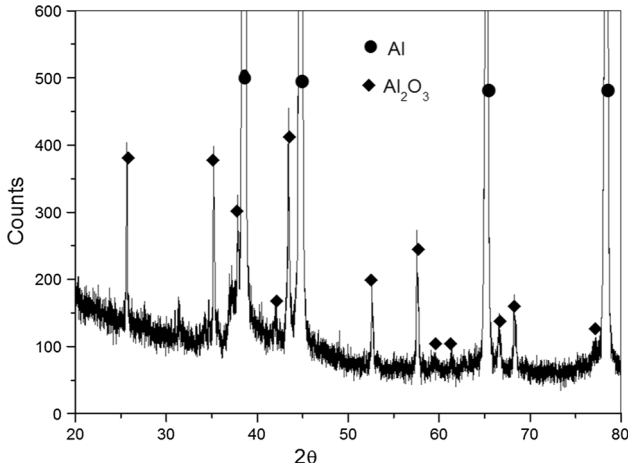

Fig. 3 X-ray diffraction of Al-1.5B-7.6 Al_2O_3 master alloy

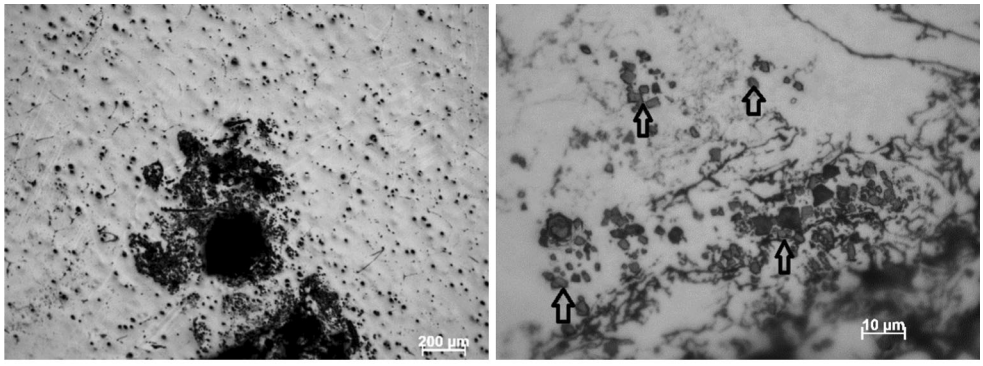

Fig. 2 Optical micrographs of Al-B2O3 mix prepared by method 1 or 2 (a) large agglomeration present in the microstructure and (b) reaction products observed near the agglomerate (shown by arrows)

that around 60% of the particles tested (total 2000 no) lie between 1 and 3 μm and 90% of the particles has a size between 1 and 9 μm. Average particle size of Al_2O_3 was calculated to be 1.8 μm from the analysis. Similarly, the area/volume fraction of the particles in the microstructure was calculated to be 27%, which is considerably higher than the calculated volume fraction from reaction 1, i.e., 5.9%. It is known that for a given mass fraction, area fraction increases with increase in number of particles because of the increase in the total surface area of particles.

4.2 Mechanism of In Situ Al_2O_3 Formation

During the introduction of liquid B_2O_3 into the molten Al-Mg alloy, low surface tension (aided by Mg) accompanied by downward force created by vortex provides the conditions for good and stable mixing. This is enough for B_2O_3 to establish reactive wetting with Al. The impeller mixing and ultrasonication result in the disintegration of liquid B_2O_3 releasing more surface area for the reaction. The influence of ultrasonication on the dispersion of ultrafine particles in molten metal was widely studied (Ref 21-23). Also the formation, growth and implosion of cavitation bubbles during the alternate acoustic pressure wave cycles were observed in detail. Bubble implosion is a violent process producing pressure pulses (~1-5 GPa), temperature spikes (>4000 °C), and high velocity jets (100 m/s) in the liquid (Ref 21). According to well-developed views, the cavitation threshold pressure is governed by the presence of cavitation nuclei such as vapor and gas bubbles, solid gas-absorbing suspensions, and hydrophobic inclusions (oxides) (Ref 21). It was experimentally demonstrated that the cavitation threshold pressure reduced from 800 to 550 kPa with the increase in alumina concentration in an aluminum melt from 0.005 to 0.1 wt.% (Ref 21). Further, the pressure sources the disintegration of intermetallics or particle agglomerates when present in the cavitation zone, depending on the threshold intensity required for the disintegration according to the equation (Ref 24)

$$I = 2W_l\left(\frac{\sigma_{stp}}{D\omega\rho_l}\right)^2 \quad \text{(Eq 4)}$$

where W is the ultrasonic power, ω is oscillation frequency, σ_{stp} is the tensile strength of particle or agglomerate, ρ is the density of the liquid, D is the diameter of particle or agglomerate. Normally, the tensile strength of agglomerate is many order lower than the monolithic particle, so it is easy to disintegrate with a low stress. For example, Al_2O_3 monolithic particle has a tensile strength of ~500 MPa, whereas micron-sized Al_2O_3 agglomerates have a strength of ~75 MPa (Ref

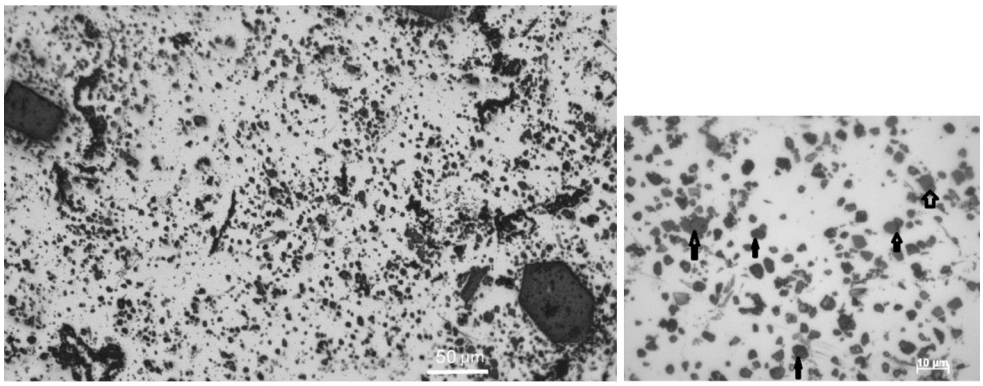

Fig. 4 (a, b) Optical micrographs of Al-1.5B-7.6Al_2O_3 prepared by method 3 (Al_2O_3 particles are represented by arrows in Fig. 4b)

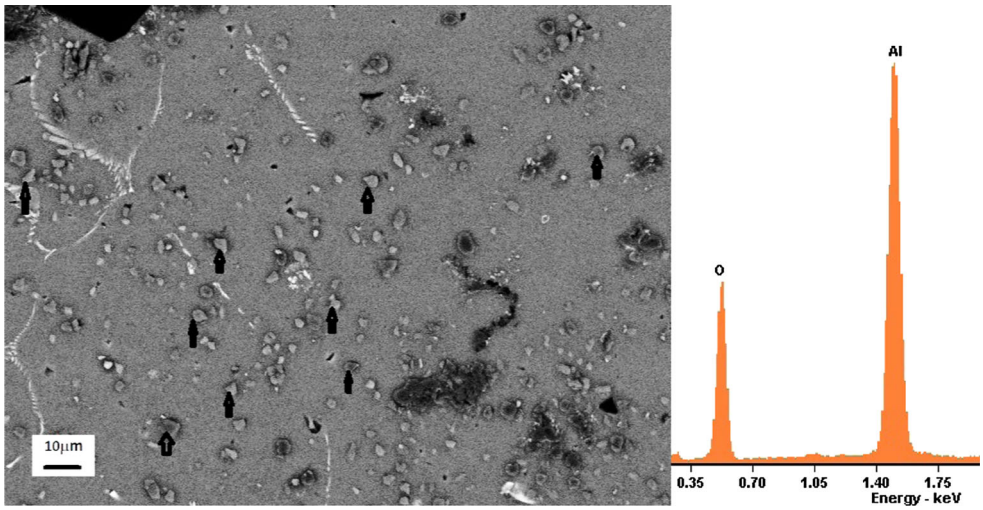

Fig. 5 Al_2O_3 phases (shown by arrows) distribution in backscattered SEM of Al-1.5B-7.6 Al_2O_3 prepared by method 3

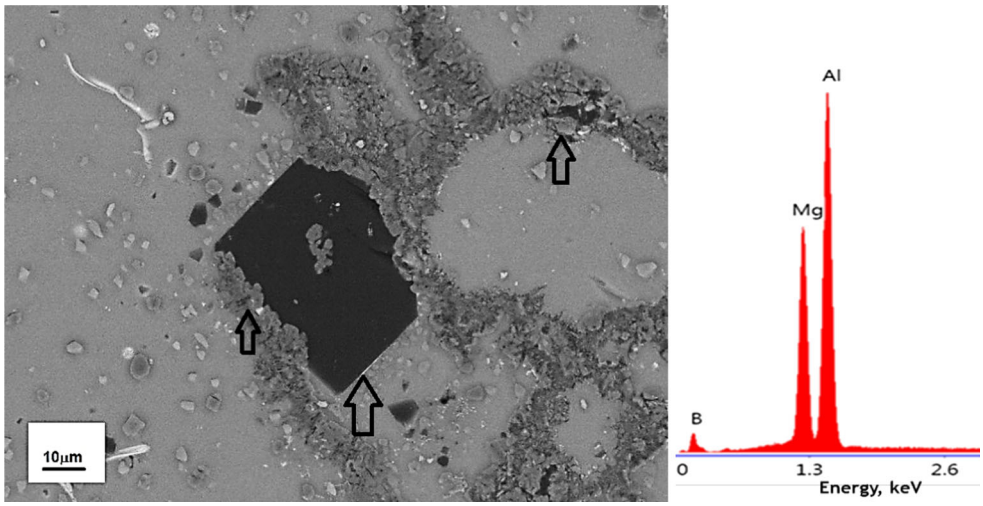

Fig. 6 Al-Mg-B phase (dark blocky crystal shown by arrow) in backscattered SEM of Al-1.5B-7.6 Al_2O_3 prepared by method 3

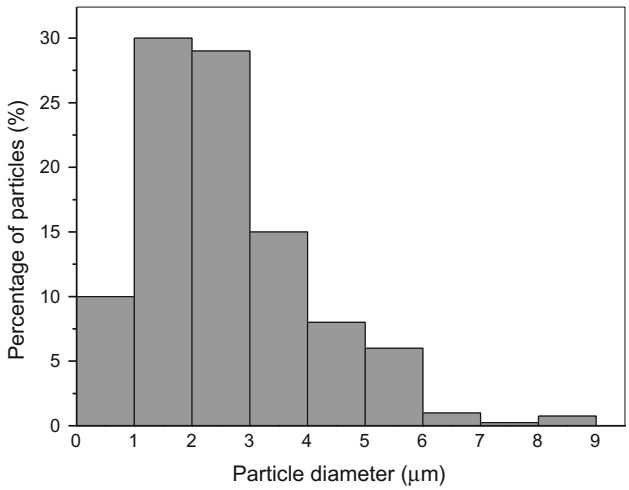

Fig. 7 Al_2O_3 particle size distribution in Al-1.5B-7.6Al2O3 master alloy

25). In the present experimental conditions, reaction products are loosely held with the liquid B_2O_3 by surface tension and cavitation pressure must be able to disintegrate the liquid to smaller droplets and de-agglomerate the product clusters at a low pressure. However, surface area minimization can result in the coalescence of tiny droplets to form larger ones in a later stage. Since there is minimum crystallographic bonding exists within liquid B_2O_3, the reaction (1) should be fast with Al in all the cases. As a result, first layer of compound forms releasing boron to the metal. In the next stage, B reacts with Al and Mg at the interface to form transition compound. As the reaction proceeds, Mg content at the interface decreases so that Al_2O_3 becomes more favorable. Both reactions are continued simultaneously to form Al_2O_3 and Al-Mg-B compounds in the final microstructure. A reduction in Mg concentration of the alloy due to its diffusion in AlB_2 compound was identified in AlB_2 reinforced Al MMCs (Ref 20). Once the Mg concentration in the alloy is reduced to less than Al_2O_3-$MgAl_2O_4$ phase equilibrium composition (0.19 wt.%), the initially formed Mg-bearing oxide such as $MgAl_2O_4$ may also transform to Al_2O_3 freeing Mg back into the alloy. This reaction mechanism reveals the possibility of Al_2O_3 formation in Al alloy at Mg content higher than the Mg required for Al_2O_3-$MgAl_2O_4$ phase equilibrium (0.19 wt.%).

The bimodal distribution of AlB_{12} particles needs to be discussed further in view of the formation of crystals. It is very clear that there is appreciable difference in the size between small and large particles. During the mixing and dispersion process, liquid B_2O_3 is likely to be dispersed into small droplets and tiny AlB_{12} crystals are formed during the reaction. Similarly, bigger AlB_{12} crystals are formed on large droplets because the crystal growth depends on the boron concentration at the interface. Interestingly, close observations of some of the large crystals pointed toward the possibility of mechanical disintegration of large crystals into tiny ones. It was seen from the microstructures that large AlB_{12} crystals have polygonal shapes with smooth edges (face) and sharp corners. However, polygonals with irregular edges (faces) were also observed in the microstructures. This was further explained from the SEM (Fig. 8) where the large particle having irregular face (indicated with straight line) and tiny crystals was found on the vicinity of the crystal face. These tiny crystals are most likely the debris that separated from the parent crystal during the disintegration process. Some of the features like sharp cut on one of the corners (arrow 1) and a tiny crystal that was about to break out from the parent crystal (arrow 4) are most likely the signatures of mechanical disintegration. Morphologies of some of the small crystals (arrows 2 and 3) have close resemblance with the cutoff corner of the large crystal. Mechanical disintegration can be possible by the implosion of cavitation bubbles, which was previously reported for Al_3Ti intermetallic in Al (Ref 26).

AlB_{12} is stable at a temperature >975 °C or at boron concentration >44.5 wt.% according to the Al-B phase diagram (Ref 27). Maximum solubility of boron in liquid Al between 660 and 975 °C is 0.022-0.35 wt.%. So most of the boron released during the reaction stays at the interface and forms AlB_{12} compound when the local concentration reaches >44.5 wt.% or the local temperature reaches 975 °C due to the exothermic nature of the reaction. As can be understood from the experimental conditions such as temperature (700-900 °C) and boron concentration (0-1.5 wt.% max), AlB_{12} cannot be stable once formed at the interface. Hence, at holding–mixing cycles, a thermodynamic driving force exists to transform the

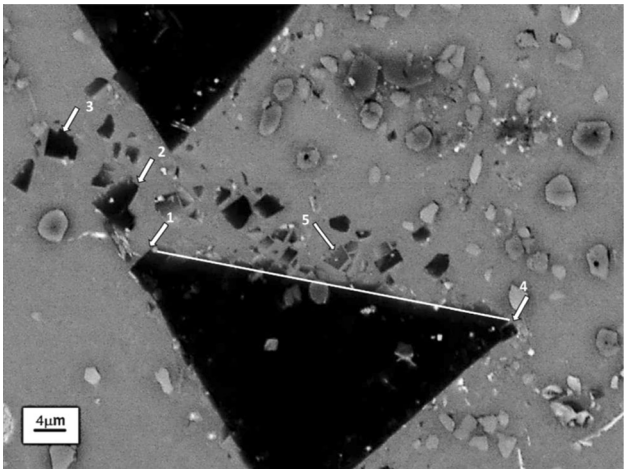

Fig. 8 SEM micrograph of Al-1.5B-7.6 Al_2O_3 master alloy (possible mechanical disintegration of the crystal is shown from the micrograph)

AlB_{12} to AlB_2. While the kinetics of transformation is sluggish for large particles, it may be quicker for tiny ones and gray particles found near the large crystal (arrow 5, Fig. 8) are possibly the transformed AlB_2 particles. In short, Al_2O_3 is detected as the most occurring phase, while AlB_{12} crystals are frequently present and AlB_2 crystals are the rarest in the master alloy. This conclusion is very much important in finding the most probable inoculant in the master alloy for the grain refinement of Al alloys (forwarding section).

A few reports on the reaction between B_2O_3 and Al (solid/liquid) are available in the literature. Birol (Ref 28) detected AlB_2 and Al_2O_3 in B_2O_3-pure Al powder mix at temperature, 875 °C, whereas AlB_{10} and Al-B-O compound started forming at a temperature, 1000 °C. Ficici et al. (Ref 29) prepared Al-AlB_2 in situ composites by the reaction between molten aluminum and B_2O_3 glass at 1400 °C. Several Al-B-O compounds were detected on the glass layer that was already floated at the top of the molten metal during the reaction. It can be inferred from the current and previous investigations that reaction between Al and B_2O_3 is complex in nature, and interestingly, different phases are formed with respect to the experimental conditions employed.

4.3 Inoculation by an Alumina-Containing Master Alloy in Al Alloys

Grain refinement potential of the master alloy (an addition level of 1 wt.%) was explored in different model Al alloys such as CPAl, Al-1Si-0.5 Mg, and commercially important Al-7Si-0.5 Mg-0.1Ti (A357) alloy. Also the influence of ultrasonication in the grain refinement was examined. Figure 9 shows the macro-etched cast billets of CPAl where large columnar grains were found in the as-cast samples (Fig. 9a, b). Columnar grains were still present in the master alloy-added samples (Fig. 9c), whereas columnar to equiaxed transition (CET) was observed in the samples ultrasonicated after the master alloy addition (Fig. 9d). The CET was further substantiated from the anodized CPAl micrographs (Fig. 10) where large columnar grains (Fig. 10a) were found to transform into equiaxed and smaller grains with the addition of the master alloy and ultrasonication treatment (Fig. 10b). In Al-1Si-0.5 Mg alloy, the large equiaxed grains with 600 ± 23 μm in size were present in the reference sample (Fig. 11). After master alloy addition, the grain size was reduced to 400 ± 12 μm and the ultrasonication helped in reducing the size to 240 ± 12 μm (Fig. 12). Figures 13, 14, and 15 show the microstructures of A357 alloy inoculated with master alloy. It is very clear that 1 wt.% of the master alloy reduced the grain size of A357 from 900 ± 30 μm (Fig. 13a) to 400 ± 19 μm (Fig. 14a). With the application of ultrasonication, the grain size was drastically reduced to 190 ± 10 μm in the master alloy-added alloy (Fig. 14b). In order to understand the significance of minimal addition of the master alloy in comparison with the commercially important grain refiner Al-5Ti-1B, the addition was reduced to 0.1 wt.% (Fig. 15). The grain size was reduced from 900 ± 30 to 500 ± 20 μm with the master alloy addition (Fig. 15a) and further reduction to 210 ± 15 μm with the application of ultrasonication (Fig. 15b). It is very clear from the results that the master alloy is able to reduce the grain size of the alloy and the ultrasonication aids the refinement further.

Figure 16 presents the cooling curves of A357 alloy inoculated with 1 wt.% of the master alloy. The alloys were cast in the same metallic mold (Fig. 1) to measure the undercooling and the nucleation temperature of the primary Al grains and understand the heterogeneous nucleation mechanism of oxide inoculant. From the thermal analysis (Fig. 16), the nucleation temperature (T_n) of primary Al crystals is identified from the first derivative of temperature ($dT/dt - t$) curve, where the slope of the T–t curve starts to deviate (Ref 30). Other two temperatures are (a) T_{min}, unsteady state growth temperature, or the onset of recalescence, where the latent heat liberated during nucleation surpasses the heat extracted from the sample and (b) T_g, the end of recalescence or the onset of steady state growth of primary α-Al dendrites. Consequently, the undercooling is approximated as $\Delta T = (T_g - T_{min})$ as in the case of the primary α-Al nucleation (Ref 30). From Fig. 16(a), the Al primary phase started nucleating at 620 °C and ended at 618.5 °C in the reference alloy (the alloy without master alloy addition). The maximum nucleation undercooling from the recalescence was calculated to be 1.5 °C. In the presence of the master alloy in A357 alloy, nucleation of Al was found to start slightly above 620 °C and no recalescence was noticed in the cooling curve (Fig. 16b). The sharp peak found in the differential curve (Fig. 16a) further confirmed the presence of recalescence in A357 Alloys which was absent in the inoculated alloy (Fig. 16b). The absence of recalescence is not uncommon in inoculated Al alloys at moderate cooling rates, 2 °C/s (Ref 31, 32). This happens due to the increased number of heterogeneous nucleation events aided by numerous nucleant particles present in the alloy. The results of thermal analysis testify that master alloy contains potent nucleants for heterogeneous nucleation of α-Al. Note that the limitations of data acquisition and thermocouple sensitivity can sometimes neglect a small change in the temperature.

Nucleation potency and efficiency of substrates are the important parameters to describe grain refinement of tested alloys; other parameters like cooling rate and composition are kept constant. The potency of a solid substrate in a liquid metal can be defined as the degree of lattice matching across the interface between the substrate and the solid phase to be nucleated. The lattice misfit f can be used as a quantitative measure of the potency for heterogeneous nucleation and is defined as $f = (dS - dN)/dS$, where dS and dN are the atomic spacing along a close-packed direction on a close-packed plane of the solid and the nucleating substrate, respectively (Ref 33).

Fig. 9 Macro-etched CPAl (a) without master alloy addition and ultrasonication, (b) with out master alloy addition and with ultrasonication, (c) with master alloy addition and without ultrasonication, (d) with master alloy addition and ultrasonication

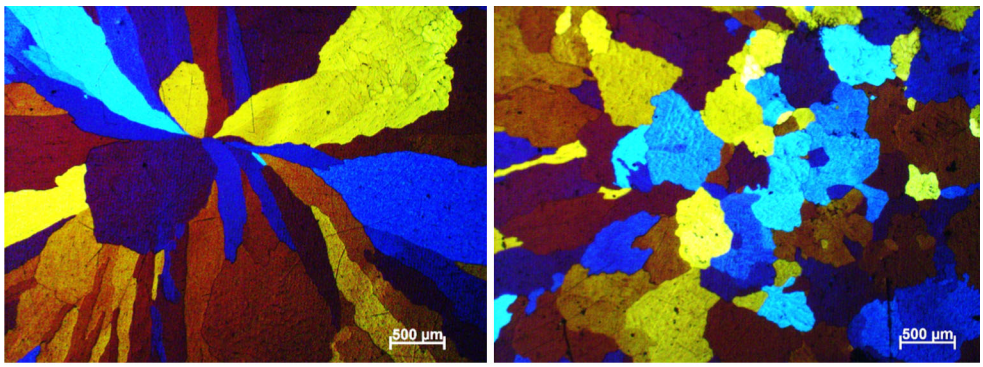

Fig. 10 Anodized micrographs of CPAl cast (a) without master alloy addition and ultrasonication and (b) with master alloy addition and ultrasonication

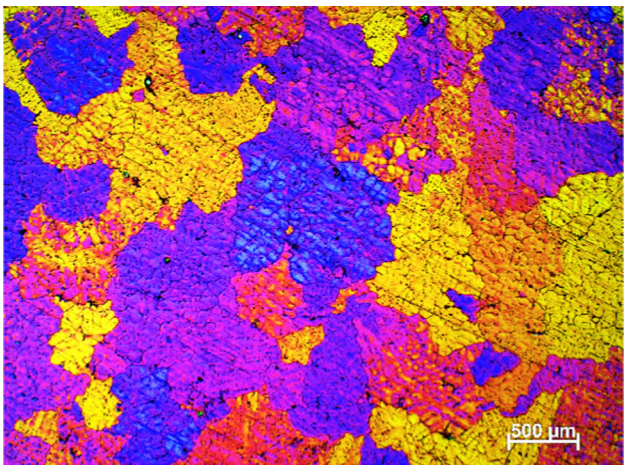

Fig. 11 Anodized micrographs of Al-1.5Si-0.5 Mg alloy cast without ultrasonication

The calculated lattice misfit with solid Al at 660 °C is 3.38% for γ-Al_2O_3 and –0.48% for α-Al_2O_3, indicating that these oxides are highly potent for nucleation of α-Al in consideration of the corresponding lattice misfit being –4.22% for TiB_2 (Ref 33). Lattice misfit for AlB_2 (−5.1%) is quite similar to that of TiB_2, and AlB_{12} displays huge misfit with α-Al (115%) (Ref 34, 35). This suggests that AlB_2 is potent nucleant, but AlB_{12} not. Nucleation efficiency refers to the effectiveness of a given type of inoculant with specific physical characteristics and solidification conditions, such as number density, size distribution and cooling rate. For example, TiB_2 particle population in an Al-5 wt.% Ti-1 wt.% B master alloy was estimated to be 10^8 particles/cm^3 with average particle size of 1 µm (Ref 35). Similarly, for the Al_2O_3 particles with average particle size 2 µm, the number density was approximated to 10^{11} particles/cm^3. According to the athermal heterogeneous nucleation theory, the nucleation and growth of the solid phase are not only related to the geometry of the nucleant particles, but also are determined by the undercooling, ΔT_g, by the equation

$$\Delta T_g = 4\,\Gamma_{sl}/D \qquad \text{(Eq 5)}$$

where Γ_{sl} is the Gibbs–Thomson coefficient between the stable embryo of the solid phase and the liquid and D is the diameter of the particle. For an Al alloy, Γ_{sl} is about 9.12×10^{-8} °C m (Ref 36). In the present study, undercooling required for Al_2O_3 to nucleate aluminum was calculated to be in the range of 0.36-0.04 °C for 1-9 µm and more 60% of the particles are >1.8 µm ($\Delta T_g < 0.2$ °C). In the present study, Al_2O_3 is qualified to be a possible nucleant for the grain refinement of α-Al.

AlB_2 is successfully used as an efficient inoculant for high Si-containing Al alloys more than 4 wt.% Si (Ref 37). Further, good grain refinement was demonstrated in Al-7Si alloy with the addition of Al-B master alloy containing AlB_2 and AlB_{12} compounds (Ref 35). All of the studies speculated a possibility of transformation of AlB_{12} to AlB_2 in the inoculation condition, but was not proved experimentally. According to the eutectic theory by Mohanty and Gruzelski, Al-B constitutes a eutectic at 0.022 wt.% B and 659.7 °C (Ref 38). A lower addition of boron (<0.022 wt.%) results in the dissolution of AlB_2 and no nucleant will be available for heterogeneous nucleation, which

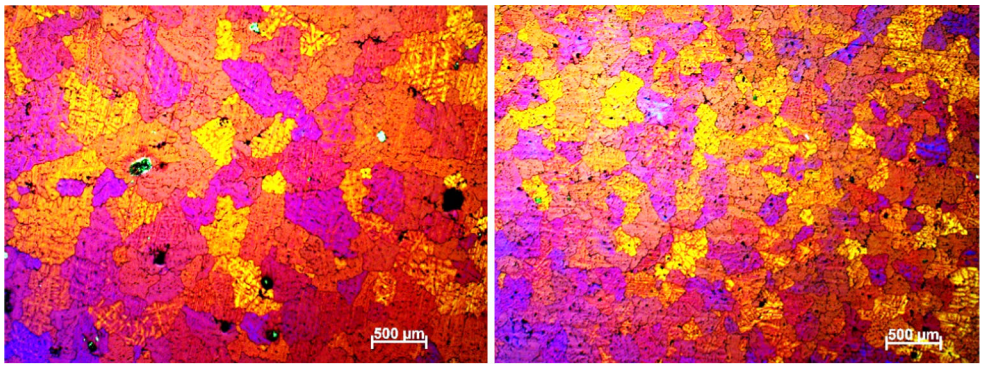

Fig. 12 Anodized micrographs of Al-1.5Si-0.5 Mg + 1 wt.% MA cast (a) without ultrasonication and (b) with ultrasonication

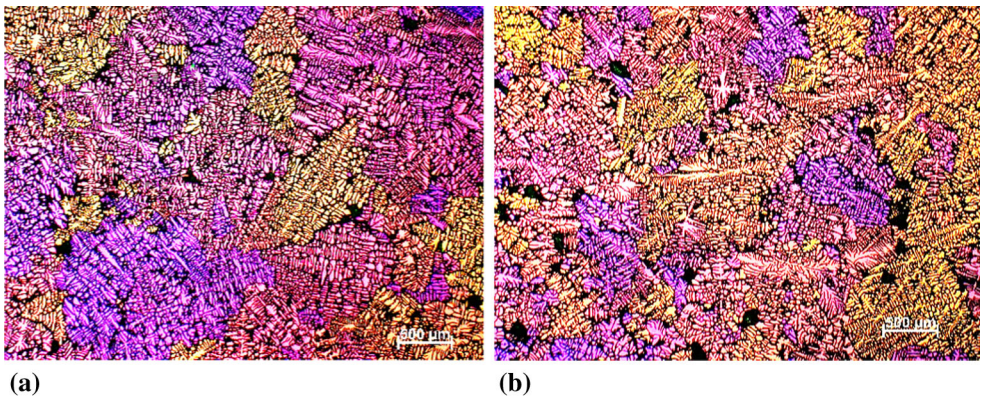

Fig. 13 Anodized micrographs of A357 cast (a) without ultrasonication and (b) with ultrasonication

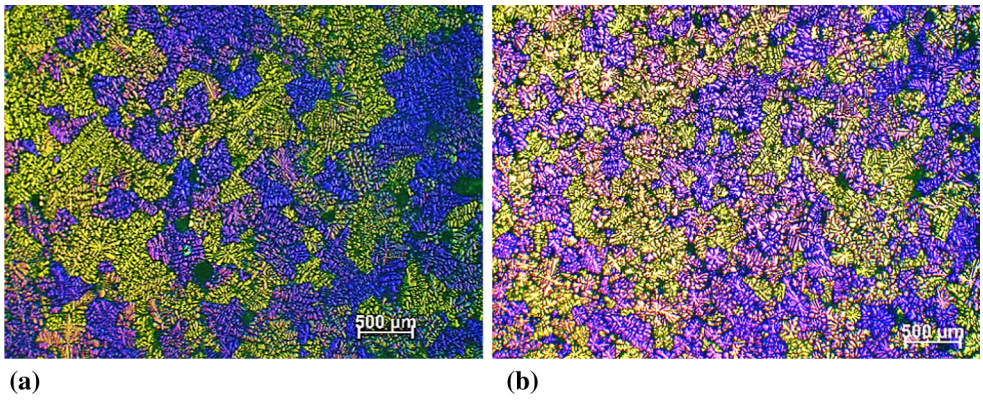

Fig. 14 Anodized micrographs of A357 + 1 wt.% MA and cast (a) without ultrasonication and (b) with ultrasonication

holds true for low Si-containing Al alloys (liquidus is near 659 °C. However, new AlB_2 precipitates in the alloy may act as nucleants in the Al-Si alloys containing more than 4 wt.% Si (liquidus is <659 °C). The dissolution–precipitation mechanism explained for AlB_2 doesn't hold true for AlB_{12} as the compound remains undissolved at longer period of time, which is substantiated in the present study. AlB_2 seems to be the rarest compound in the present study, which negates the possibility of it being an active nucleant for grain refinement. 1 wt.% of master alloy is equivalent to 0.015 wt.% Boron in the master alloy, which is less than the eutectic point of Al-B. It is confirmed by many investigators that grain refinement is insignificant in Al-7Si alloy at boron concentration less than 0.022 wt.% (Ref 35, 39, 40). But the current study explicitly showed that the master alloy is capable of reducing the grain size of Al-7Si alloy even at a boron concentration of 0.0015 wt.% (0.1 wt.% MA) (Fig. 15). This underlines the fact that the influence of Al_2O_3 particles in the enhancement of grain refinement is substantial.

The influence of ultrasonication close to the liquidus temperature on the grain refinement of alloys was studied extensively (Ref 21). A systematic study by Wang et al. (Ref 41) in a non-inoculated alloy made clear that ultrasonication in complete liquid state had negligible effect on grain

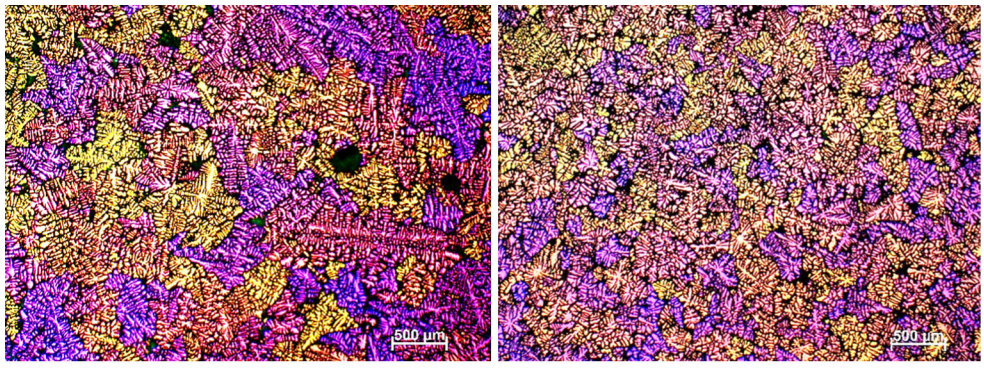

Fig. 15 Anodized micrographs of A357 + 0.1 wt.% MA and cast (a) without ultrasonication and (b) with ultrasonication

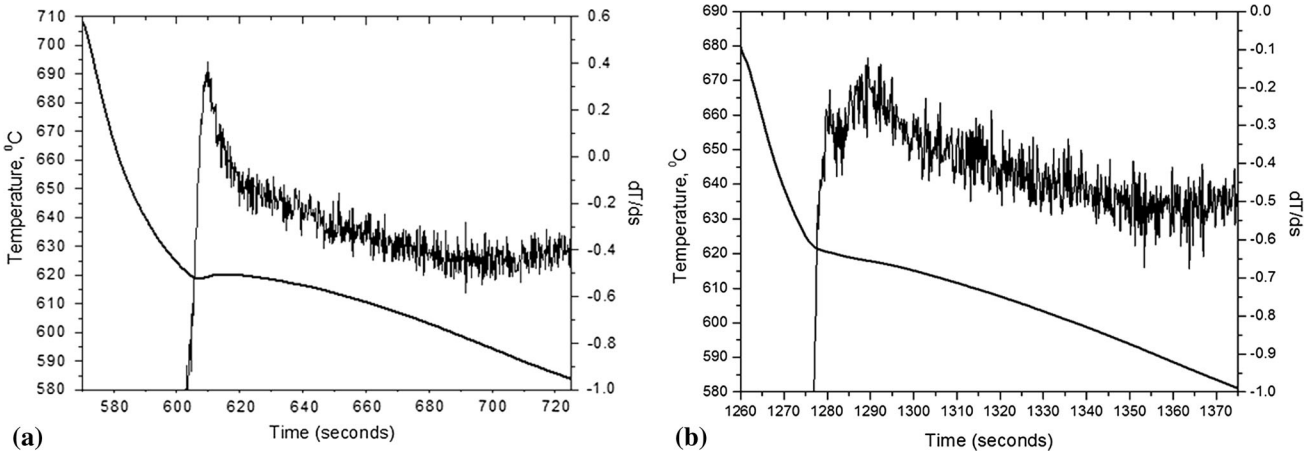

Fig. 16 Cooling curves of (a) A357 and (b) A357 inoculated with 1 wt.% MA

refinement, which is substantiated in recent studies by the authors (Fig. 9b, 13). It is important to note that ultrasonication gives additional grain refinement benefit when applied to the liquid metal containing inoculant particles. Manual stirring or mechanical stirring found to fail in distributing fine particles in liquid metal. Cavitation and associated acoustic streaming seem to be contributing to the distribution of inoculant particles within the metal ensuring more particles for the nucleation event. Recent work showed that ultrasonication is capable of dispersing in situ $MgAl_2O_4$ particulates in liquid metal (Ref 5, 18). It is clear from the microstructure analysis that the master alloy obtained in the current work contains homogeneously distributed Al_2O_3 (see Fig. 4). During the addition of master alloy in molten Al, Al_2O_3 immediately comes in contact with the dissolved hydrogen. It was experimentally proved that alumina particles are active absorbent of hydrogen and stabilize the absorbed hydrogen on the surface of the particles. This may eventually prevent the potential crystallographic planes to come in contact with Al for nucleation. Further, fine particles show a tendency to agglomerate due to the Vander Waals force, which in turn reduce the number density of the particles. Altogether, the nucleation potency and efficiency are negatively affected by both phenomena. During the ultrasonication treatment with an intensity higher than the cavitation threshold, cavitation bubbles are nucleated and grown on the particle surface. High energy pulsation and jet created during the bubble implosion disintegrate the particle agglomerates and strip off the gaseous layer, given that the nucleating surfaces are again accessible to the molten metal. This explanation is illustrated by the microstructures in Fig. 17, where a large cluster of particles is observed in the non-ultrasonicated A357 alloy, while clusters are smaller after ultrasonication. Interestingly, clustered particles are found inside α-Al in both the cases. Columnar to equiaxial transition observed in CPAl and additional grain size reduction in other studied alloys signify the improvement in the potency and efficiency of Al_2O_3 particles after ultrasonication.

4.4 Mechanical Properties

It is essential to testify the performance of a grain refiner in terms of the mechanical performance of the inoculated alloys. Figure 18 shows the tensile testing performance of aged A357 alloy inoculated with 1 wt.% of the master alloy. The stress–strain graphs of different alloys are denoted as 1, 2, 3, and 4. The yield strength, UTS, and elongation of the reference alloy (Fig. 18-1) were found to increase after the ultrasonication treatment (Fig. 18-2). The alloy inoculated with the master alloy showed an improvement in yield strength and UTS, but an appreciable reduction in elongation most likely due to the particle agglomeration and associated defects was noticed (Fig. 18-3). The ultrasonication seemed to help in the improvement in elongation and UTS of inoculated alloy (Fig. 18-4). However, no difference in the yield strength was noticed in both the inoculated alloys.

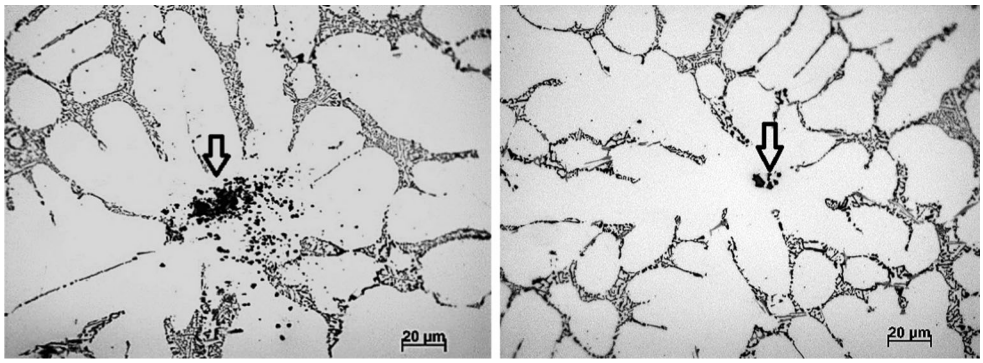

Fig. 17 Optical micrographs of A357 + 1 wt.% MA (a) without ultrasonication and (b) with ultrasonication (particle clusters are shown by arrows)

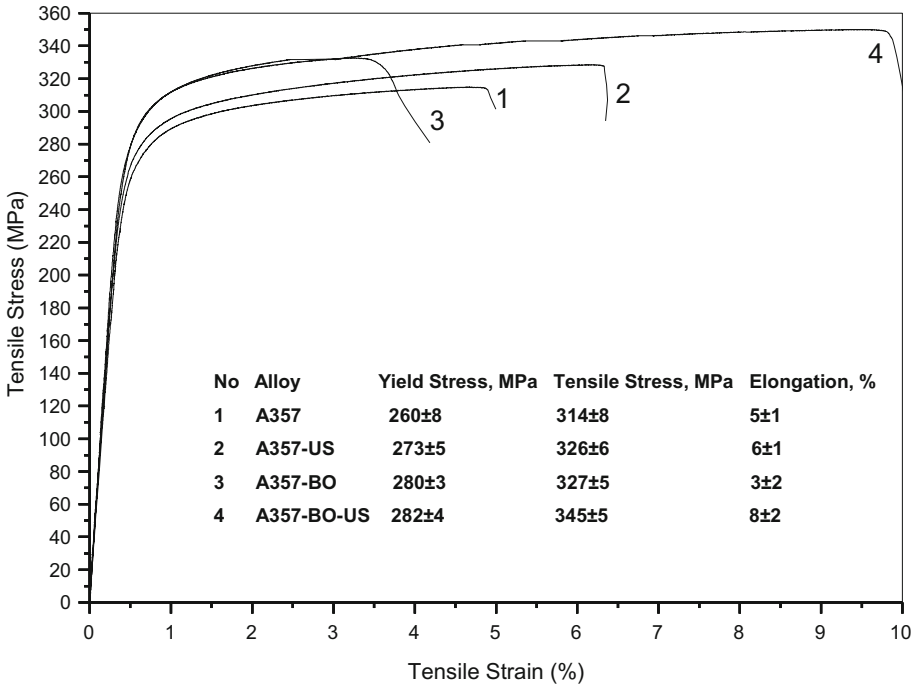

Fig. 18 Tensile stress–tensile strain curves of A357 alloys inoculated with Al-1.5B-7.6Al2O3 master alloy and treated with ultrasonication. The values are given in a table inside the figure

5. Conclusion

In situ α-Al_2O_3 dispersed Al composite master alloy was prepared using B_2O_3 and ultrasonication-aided liquid metallurgy route. α-Al_2O_3, AlB_{12}, and AlB_2 compounds were identified in the master alloy, where α-Al_2O_3 was most commonly observed in the microstructure. Detailed microstructure analysis identified Mg atom diffusion in AlB_{12} compound and a possible transformation of AlB_{12} to AlB_2. Al_2O_3 particles of size between 1 and 9 µm were largely found in the microstructure. The grain refinement potential of the master alloy was successfully tested in model and commercial Al alloys. With the combination of master alloy addition and ultrasonication, CET transition was observed in CPAl and 75% reduction in the grain size was achieved in A357 alloy. A detailed analysis identified the role of α-Al_2O_3 as nucleating substrate for the refinement of α-Al in the alloys. The ultrasonication treatment distributes the Al_2O_3 particles that subsequently provide enhanced heterogeneous nucleation events during solidification, resulting in the grain refinement of both CP Al and A357 alloys. A357 alloys exhibited an improvement in strength and ductility after inoculation and ultrasonication treatment.

Acknowledgment

The authors wish to acknowledge financial support from the ExoMet Project, which is co-funded by the European Commission in the 7th Framework Programme (Contract FP7-NMP3-LA-2012-280421), by the European Space Agency and by the individual partner organizations.

References

1. R. Asthana, *Solidification Processing of Reinforced Metals*, Trans Tech Publications Ltd, Zurich, 1998
2. P.K. Rohatgi, R. Asthana, and S. Das, Solidification, Structures, and Properties of Cast Metal-Ceramic Particle Composites, *Int. Metals Rev.*, 1986, **31**(1), p 115–139
3. G. Ramani, R.M. Pillai, B.C. Pai, and T.R. Ramamohan, Factors Affecting the Stability of Non-wetting Dispersoid Suspensions in Metallic Melts, *Composites*, 1991, **22**(2), p 143–150
4. T.P.D. Rajan, R.M. Pillai, and B.C. Pai, Reinforcement Coatings and Interfaces in Aluminium Metal Matrix Composites, *J. Mater. Sci.*, 1998, **30**, p 3491–3503
5. V.M. Sreekumar, N. Hari Babu, D.G. Eskin, and Z. Fan, Structure–Property Analysis of In Situ Al-MgAl2O4 Metal Matrix Composites Synthesized Using Ultrasonic Cavitation, *Mater. Sci. Eng. A*, 2015, **628**, p 30–40
6. Y. Le Petitcorps, J.M. Quenisset, G. Le Borgne, and M. Bathole, Segregation of Magnesium in Squeeze-Cast Aluminium Matrix Composites Reinforced with Alumina Fibres, *Mater. Sci. Eng. A*, 1991, **135**, p 37–40
7. Y. Kim and J.C. Lee, Processing and Interfacial Bonding Strength of 2014 Al Matrix Composites Reinforced with Oxidized SiC Particles, *Mater. Sci. Eng. A*, 2006, **420**, p 8–12
8. M.O. Lai, L. Lu, and B.Y. Chung, Formation of Mg-Al-Ti/MgO Composite Via Reduction of TiO2, *Compos. Struct.*, 2002, **57**, p 183–187
9. G. Chen, G.X. Sun, and Z.G. Zhu, Study on Reaction-Processed Al-Cu-AlB2-BOB3B (p) Composites, *Mater. Sci. Eng. A*, 1999, **265**, p 197–201
10. V.M. Sreekumar, *On the Formation of Magnesium Aluminates Spinels* In Situ *in Molten Aluminium–Magnesium Alloys Mixed with Silica Particles*, Ph.D. thesis, Indian Institute of Technology, Kharagpur, 2008
11. D. Horvitz and I. Gotman, Pressure-Assisted SHS Synthesis of MgAl2O4–TiAl In Situ Composites with Interpenetrating Networks, *Acta Mater.*, 2002, **50**, p 1961–1971
12. V.M. Sreekumar, K.R. Ravi, R.M. Pillai, B.C. Pai, and M. Chakraborty, Thermodynamics and Kinetics of the Formation of Al2O3/MgAl2O4/MgO in Al-Silica Metal Matrix Composite, *Metall. Mater. Trans. A.*, 2008, **39**, p 919–933
13. M. Hanabe and P.B. Aswath, Synthesis of In Situ Reinforced Al Composite from Al-Mg-Si-O Precursors, *Acta Mater.*, 1997, **45**, p 4067–4076
14. D. Horvitz, I. Gotman, E.Y. Gutmanas, and N. Claussen, In Situ Processing of Dense Al2O3–Ti Aluminide Interpenetrating Phase Composites, *J. Eur. Ceram. Soc.*, 2002, **22**, p 947–954
15. T.V. Atamanenko, D.G. Eskin, L. Zhang, and L. Katgerman, Criteria of Grain Refinement Induced by Ultrasonic Melt Treatment of Aluminum Alloys Containing Zr and Ti, *Metall. Mater. Trans. A*, 2010, **41**, p 2056–2066
16. H.T. Li, Y. Wang, and Z. Fan, Mechanisms of Enhanced Heterogeneous Nucleation During Solidification in Binary Al-Mg Alloys, *Acta Mater.*, 2012, **60**, p 1528–1537
17. K. Kim, The Effect of Melt Conditioning on Segregation of Solute Elements and Nucleation of Aluminum Grains in a Twin Roll Cast Aluminum Alloy, *Metall. Mater. Trans. A*, 2014, **45**(10), p 4538–4548
18. V.M. Sreekumar, N.H. Babu, D.G. Eskin, and Z. Fan, Development of New Oxide Based Master Alloys and their Grain Refinement Potency in Aluminium Alloys, *Mater. Sci. Forum*, 2015, **828-829**, p 23–28
19. Ömer Savas and Ramazan Kayikci, A Taguchi Optimisation for Production of Al-B Master Alloys Using Boron Oxide, *J. Alloys Compd.*, 2013, **580**, p 232–238
20. H.E. Calderón, R.G.I. Hidalgo, Z.H. Melgarejo, and O.M. Suárez, Effect of AlB2–Mg Interaction on the Mechanical Properties of Al-based Composites, *Mater. Sci. Eng. A*, 2010, **527**, p 2258–2264
21. G.I. Eskin and D.G. Eskin, *Ultrasonic Treatment of Light Alloy Melts*, 2nd ed., CRC Press, Boca Raton, 2014
22. O.V. Abramov, *Ultrasound in Liquid and Solid Metals* (Boca Raton, CRC Press, 1994), pp. 43–77, 273–406
23. K.S. Suslick and G.J. Price, Applications of Ultrasound to Materials Chemistry, *Annu. Rev. Mater. Sci.*, 1999, **29**, p 295–326
24. O. Kudryashova and S. Vorozhtsov, On the Mechanism of Ultrasound-Driven Deagglomeration of Nanoparticle Agglomerates in Aluminum Melt, *J. Met.*, 2016, **68**(5), p 1307–1311
25. A.V. Timoshkin. Integrated Refining and Modifying of Silumins by Method of High-Speed Jet Melt Processing (in Russian; Moscow, 2003)
26. F. Wang, D.G. Eskin, T. Connolley, and J. Mi, Effect of Ultrasonic Melt Treatment on the Refinement of Primary Al_3Ti Intermetallic in an Al-0.4Ti Alloy, *J. Cry Growth*, 2016, **435**, p 24–30
27. O.N. Carlson, Al-B Phase Diagram, *Bull. Alloy Phase Diagr.*, 1990, **11**(6), p 560–566
28. Y. Birol, Aluminothermic Reduction of Boron Oxide for the Manufacture of Al-B Alloys, *Mater. Chem. Phys.*, 2012, **136**, p 963–966
29. F. Ficici, S. Koksal, Rn Kayikci, and O. Savas, Investigation of Unlubricated Sliding Wear Behaviour of In Situ AlB2/Al Metal Matrix Composite, *Adv. Compos. Lett.*, 2011, **20**(4), p 109–116
30. M. Nowak, L. Bolzoni, and N. Hari Babu, Grain Refinement of Al-Si Alloys by Nb-B Inoculation. Part I: Concept Development and Effect on Binary Alloys, *Mater. Des.*, 2015, **66**, p 366–375
31. S.M. Jigajinni, K. Venkateswarlu, and S.A. Kori, Computer Aided Cooling Curve Analysis for Al-5Si and Al-11Si Alloys, *Int. J. Eng. Sci. Technol.*, 2011, **3**(6), p 257–272
32. V. Gutiérrez, G. González, and A. García, Thermal Analysis of Grain Refinement and Modification of an A356 Cast Alloy, *Chem. Mater. Res.*, 2014, **6**(6), p 52–62
33. M.X. Zhang, P.M. Kelly, M.A. Easton, and J.A. Taylor, Crystallographic Study of Grain Refinement in Aluminum Alloys Using the Edge-to-Edge Matching Model, *Acta Mater.*, 2005, **53**, p 1427–1438
34. S. Nafisi and R. Ghomashchi, Boron-Based Refiners: Implications in Conventional Casting of Al-Si Alloys, *Mater. Sci. Eng. A*, 2007, **452–453**, p 445–453
35. T.E. Quested and A.L. Greer, The Effect of the Size Distribution of Inoculant Particles on As-Cast Grain Size in Aluminium Alloys, *Acta Mater.*, 2004, **52**, p 3859–3868
36. J.A. Dantzig and M. Rappaz, *Solidification*, CRC Press, Boca Raton, 2009
37. Y. Birol, Effect of Silicon Content in Grain Refining Hypoeutectic Al-Si Foundry Alloys with Boron and Titanium Additions, *Mater. Sci. Technol.*, 2012, **28**(4), p 385–389
38. P.S. Mohanty and J.E. Gruzleski, Grain Refinement Mechanisms of Hypoeutectic Al-Si Alloys, *Acta Mater.*, 1996, **44**, p 3749–3760
39. P.A. Tondel and G. Halvorsen, Grain Refinement of Hypoertectic Al-Si Foundry Alloys by Addition of Boron Containing Silicon, *Light Metals*, S.K. Das, Ed., TMS, Denver, CO, 1993, p 783–790
40. L. Yuan, D. Chao, and L.Y. Xiang, Grain Refining Mechanism of Al-3B Master Alloy on Hypoeutectic Al-Si Alloys, *Trans. Nonferrous Met. China*, 2011, **21**, p 1435–1440
41. G. Wang, M.S. Dargusch, M. Qian, D.G. Eskin, and D.H. StJohn, The role of Ultrasonic Treatment in Refining the As-Cast Grain Structure During the Solidification of an Al-2Cu Alloy, *J. Cryst. Growth*, 2014, **8**, p 119–124